

PREDICTION OF STRESS CORROSION
CRACKING IN 304 STAINLESS STEEL
CANISTERS IN DRY STORAGE OF SPENT
FUEL BY MODELING: ANALYSIS OF WELD
RESIDUAL STRESS AND SUSCEPTIBLE
MICROSTRUCTURE

S. GORDON*, X. WU*, Z. YU* and S. LIU*

**George S. Ansell Department of Metallurgical and Materials Engineering
Center for Welding, Joining and Coatings Research
Colorado School of Mines, Golden, CO 80401, U.S.A.*

DOI 10.3217/978-3-85125-615-4-12

ABSTRACT

Atmospheric chloride-induced stress corrosion cracking (CISCC) in the weldments of spent fuel canisters is one of the primary safety concerns during the dry storage of used nuclear fuel at Independent Spent Fuel Storage Installations (ISFSI) in coastal areas. For SCC to occur, three criteria must be met: an aggressive chemical environment, susceptible microstructure, and sufficient tensile stress. Instead of the environment, this paper will focus only on the material microstructure and stress state. Firstly, finite element analysis (FEA) based numerical simulation models were developed for the welding of the mockup canister. Multi-pass arc welding process was considered. The thermal history and residual stress distribution induced by the longitudinal, circumferential, and the intersection between longitudinal and circumferential welds were developed based on a thermal-mechanical coupling model using ABAQUS software. The simulation results were compared with the deep-hole drilling (DHD) and contour measurement data. Based on the model-predicted stress results, a four-point bend (4PB) setup was then designed to duplicate the weld residual stress onto the 4PB specimen, on which the maximum tensile stress is close to the predicted maximum stress level of 250 MPa in the weld heat-affected zone (HAZ). A stress gradient also existed along the thickness of the 4PB specimen which allowed for the consideration of stress variation. The designing of the 4PB test was done by FEA method using ABAQUS software, and verified by digital image correlation (DIC) measurements. Besides, to identify the most susceptible microstructure of the canister to corrosion under the weld residual stress in the controlled environment, the modified implant test (CEMIT) was designed. A FEA model considering the welding process and the following uniaxial tensile load was then developed using the SYSWELD software. The residual stress and thermal history were obtained during and after the CEMIT welding process, and after the uniaxial tensile loading process. These tests yielded instructive information for the prediction of the initiation site of the crack. The initiation of the crack observed in the experiments was explained based on the simulation data. While each of the three simulations provided an independent story, the three together produced a complete

Mathematical Modelling of Weld Phenomena 12

and complementary picture. Stress corrosion cracking is a series of complex interactions which simultaneously occur. The thermal mechanical model of the canister provides information for predicting the location at which stress corrosion cracking will most likely occur. The model for the 4PB test predicts the stress gradient which occurs in a bent bar. The SYSWELD CEMIT model predicts the welding cycle, the thermal history, residual stress and loading behavior of the specimen. By design, each independent CEMIT provides the location of the most crack susceptible location under a specified environment.

Keywords: Stress corrosion cracking, Spent fuel canister, Weld residual stress, Susceptible microstructure, Modelling

INTRODUCTION

CISCC in the weldments of spent nuclear fuel (SNF) canisters is one of the primary safety concerns during the dry storage of used nuclear fuel at Independent Spent Fuel Storage Installations (ISFSI) in coastal areas [1]. For SCC to occur, three criteria must be met: an aggressive chemical environment, susceptible microstructure, and sufficient tensile stress. Field sampling analysis of surface deposits on in-service spent nuclear fuel storage canisters at three near-marine ISFSI sites in the United States have demonstrated the presence of chloride-rich salts on the canister surfaces [2-4]. As part of the surface of the canisters cools sufficiently for the salts to deliquesce, chloride-rich aqueous brine layer could form locally on the surface, leading to potential failures by CISCC in regions with high tensile stress. On the other hand, for austenitic stainless steel SNF interim canisters, the multi-pass welding procedures introduce high tensile residual stresses and sensitization in the HAZ. Therefore, the potential for CISCC in the weldments of the stainless steel interim storage canisters has been identified as a high priority data gap.

To gain fundamental understanding of the pitting and cracking behavior in the canisters and to accurately predict their long-term performance, the first step is to obtain the accurate residual stress distribution within the canisters, especially in the weldments. In the last decade, there have been several studies on the residual stresses in the canister welds. For example, Kosaki et al. [5] reported that the experimentally measured weld residual stresses were close to the yield stress through thickness on a cylindrical canister of 1.3 m in diameter and with walls approximately 75 mm thick. The Nuclear Regulatory Commission (NRC) simulated the residual stresses for typical canister welds by employing a two-dimensional, sequentially-coupled thermal-structural FE model [6], and predicted that tensile stresses of sufficient magnitude to initiate SCC are likely to be present in the HAZ of both longitudinal and circumferential welds through the wall thickness of the canisters, allowing for crack propagation through the wall thickness over time. There is very limited literature on 3D simulation of the residual stress induced by multi-pass longitudinal and circumferential welds in the dry storage fuel canisters. As for the microstructure of the canister material, possible factors that may influence the CISCC include the sensitization, ferrite, martensite, inclusions, grain size, phase orientation, texture, and so on. It is, thus, necessary to determine the most susceptible microstructure for the weld region of the canister under the influence of weld heat input and mechanical stresses. In this study, a 3D FE model using ABAQUS software was built to simulate the residual stress contours in the 304 stainless steel canisters with the presence of both longitudinal and circumferential multi-pass welds. Experimental measurements by deep hole drilling (DHD) and contour methods provide valuable comparisons with the simulation

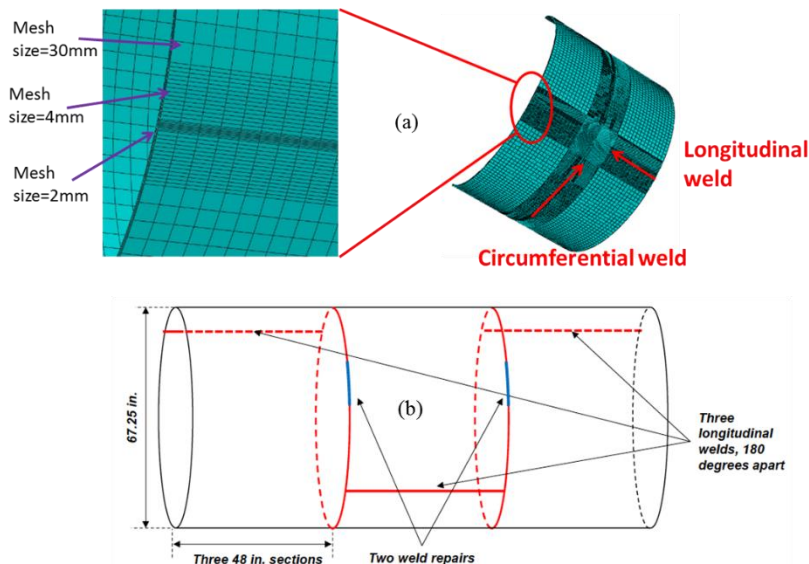
Mathematical Modelling of Weld Phenomena 12

results. Then, a modified four-point bend setup was built to duplicate the weld residual stresses into a small sample, by which subsequent corrosion tests will be carried out. At last, a modified implant test was designed, together with FEA, to characterize the most susceptible microstructure for the initiation of SCC.

SIMULATION DETAILS AND EXPERIMENTAL METHODOLOGIES

WELD RESIDUAL STRESS SIMULATION

The ABAQUS software was used to build the residual stress models for longitudinal and circumferential double-V groove multi-pass welds. Fig. 1(a) demonstrates the meshed structure with 52100 brick elements established based on the actual geometry of the mockup and the welding conditions as schematically illustrated in Fig. 1(b). The mockup consists of three cylindrical shells that were 4 feet (~1220 mm) long each and 5/8 inch (~15.9 mm) thick as shown in Fig. 1(b). The shells were rolled from a plate into a cylinder and then welded at the longitudinal seam. The three cylinders were joined together by two circumferential welds. Details of the welding parameters including pass sequence, voltage, current, travel speed and heat input for each weld pass can be found in reference [7]. Take longitudinal welds for example, the three inner passes were made first, followed by the four passes in outer diameters. Since the three longitudinal welds were arranged 180 degrees apart (see Fig. 1(b)) and the two circumferential welds were separated by the middle section, the interference between the same welding types can be negligible. Hence, in this FE model, only the longitudinal and circumferential intersecting joint in half of the mockup section was simulated, as shown in Fig. 1(a), and the welding length was sufficient to reach steady state. Note that the heat source travelled through the whole length of the welds to ensure the elements experience the same thermal history as did the actual welds.



Mathematical Modelling of Weld Phenomena 12

Fig. 1 (a) The FEA model for the mockup with fine meshes near welds, and (b) schematic drawing of the mockup.

The multi-pass weld beads have sharp transition angles, as shown in Fig. 2, which demands extremely fine meshes. More importantly, the intersecting longitudinal and circumferential welds needs compatible meshing. Due to such complications, the weld bead was divided into small rectangle-shaped areas matching the experimental bead morphology as closely as possible. The experimental bead morphology of each pass is outlined by the dotted curves in Fig. 2 and the corresponding simulation passes are highlighted in various colors. Such simplification avoided elements with sharp angles and assisted the FE model to converge more easily.

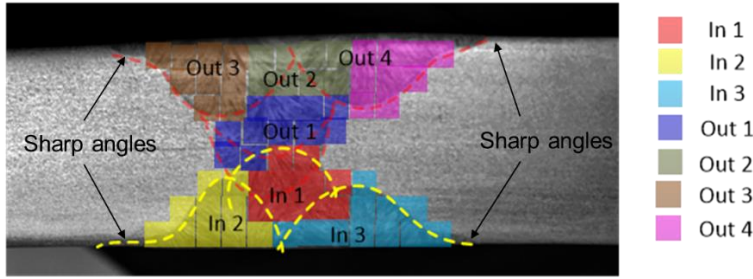


Fig. 2 Experimental bead morphology and the corresponding computational weld bead. In the figure, “in” means inner diameters of the mockup, and “out” refers to the outer diameters of the mockup.

The mockup base material is 304 stainless steel (SS). The material properties used in the simulation were taken from Deng’s work [8]. Temperature-dependent hardening modulus used in this model was obtained from Liu’s work [9]. The material solidus and liquidus temperatures were set at 1400 and 1450 °C, respectively. The latent heat of fusion was set to be 260 kJ/kg. The material properties were assumed to be the same for both base and weld metals due to lack of information in 308 weld metal physical properties.

Double-ellipsoidal heat source model developed by Goldak [10] as illustrated in Fig. 3 was used to simulate the heat input of submerged-arc welding process. The front and rear parts of the heat flux are described by Eqs. (1) and (2), respectively:

$$q_r(x, y, z) = \frac{6\sqrt{3}f_r\eta Q}{a_rbc\pi\sqrt{\pi}} \exp\left(-\frac{3x^2}{a_r^2} - \frac{3y^2}{b^2} - \frac{3z^2}{c^2}\right) \quad (1)$$

$$q_f(x, y, z) = \frac{6\sqrt{3}f_f\eta Q}{a_fbc\pi\sqrt{\pi}} \exp\left(-\frac{3x^2}{a_f^2} - \frac{3y^2}{b^2} - \frac{3z^2}{c^2}\right) \quad (2)$$

where the front and rear quadrant fractions, f_f and f_r , were set to be 0.6 and 1.4, respectively. The heat input was defined as $Q = V \cdot I \cdot \eta$, where $V = 30$ V, $I = 400$ A and $\eta = 0.8$. The constants a_f , a_r , b , and c were set to be 13, 26, 13, and 13, respectively, to closely match the experimental fusion boundary in Fig. 2.

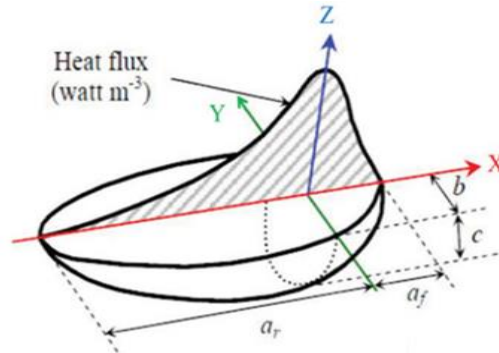


Fig. 3 Heat source model for the weld simulation.

The weld residual stresses were also characterized by DHD and contour measurement method developed by Sandia National Laboratory [7], which can be used to validate the simulation data. Detail comparison between simulation and experimental data are discussed in Section 3.

REPLICATION OF RESIDUAL STRESSES BY FOUR-POINT BENDING TEST

The stresses experienced by the mockup materials were duplicated to laboratory scale specimens through four-point bend (4PB) test. In this modified 4PB test setup, pitting initiation/growth was characterized within the thickness of the specimen, which covered stress levels from compression to tension. The maximum tensile residual stress, as indicated in another report by the same authors [11], was predicted to be around 250 MPa in the HAZ, so the design of this 4PB setup was to obtain maximum stress on the tensile side close to 250 MPa. FE method was adopted to design the geometry of this setup to allow for a sufficient sampling area within a small stress increment. Fig. 4 illustrates the finalized geometry design. The frame and actuator material is 316 stainless steel, and they were coated with Kolor-Proxy high build polyamide-epoxy primer that provides abrasion, impact and chemical resistance.

Mathematical Modelling of Weld Phenomena 12

amounts of deformation-induced martensite contributes to stress corrosion in the corrosive environment.

As a result of the high temperature, the base material near the fusion line may recover and/or recrystallize, and if near enough to the weld zone, may melt. Softening generally occurs in this region. Further away from the weld there is a region where the kinetics for carbide (Cr_{23}C_6) precipitation is favorable. The material within this region is heat treated to between 450 to 850oC and is commonly known as the sensitized region and under proper conditions can be more prone to corrosion. The upper and lower limits of the temperature range can change according to the chemical composition, in particular, carbon content, of the stainless steel. Alloys with lower carbon content will see lower temperatures and longer delay times for carbide precipitation. To account for residual stress development, a thermal mechanical model was developed to simulate the conditions in the canister during and after welding. Due to the size of the canister, the complex residual stress states, and ever changing natural environment, determining the exact location and time when SCC will happen is difficult.

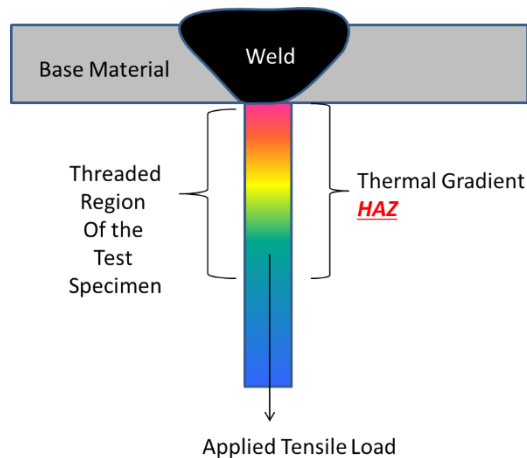


Fig. 6 A threaded cylindrical specimen with a weld bead on top. A tensile load is applied at the conclusion of the welding. The arrow indicates the direction of loading.

The Implant testing was substantially modified from its original intention [12-13] with the addition of an environmental chamber to introduce the corrosive elements (salt load, relative humidity, and temperature). To simulate the environment of the canister, salts would be deposited in the threaded region of the welded cylinder and the specimen would be placed into the chamber with preset temperature and humidity. The specimen would then be loaded to a pre-determined stress level. Under load, the notch concentrates the stress to the root of the threads. Fig. 6 shows a generalized schematic drawing depicting the basic concept of the implant test. When the specimen is provided with the proper conditions for corrosion, pitting and cracking can be observed in the notched region.

A thermal mechanical model using SYSWELD was developed to simulate the welding process for the Implant test. The thermal histories determined from both models: the canister and the Implant test can be compared. Similar thermal cycles found in the models should produce similar microstructures in both weldments (on the canister and in the Implant test). By using the thermal cycle determined from the Implant test model at the

Mathematical Modelling of Weld Phenomena 12

location in the threads where pitting corrosion and cracking occurred, a corresponding location for crack-susceptible microstructure can be determined on the model developed for the canister. Grain size as well as degree of sensitization can be used to support the microstructural behavior prediction.

By using the temperature-time profiles determined by the models, bulk material with the crack-susceptible microstructures can then be produced for testing by using the Gleeble or other heat treatment techniques. Testing of this material can lead to the determination of pitting initiation times, crack growth rates, and resistance to cracking once cracks are initiated.

For atmospheric SCC testing, the basic Implant testing equipment would be modified. However, the basic fundamentals of the test would remain the same, i.e. a welded threaded specimen is pulled in tension. The major differences are, (1) after welding, the threaded region of the specimen is coated in a corrosive media (salt loading), and (2) instead of ambient conditions, the tensile loading of the specimen is conducted under a controlled environment. By loading the end of this vertical cylindrical specimen of Type 304 stainless steel in the corrosive media, the spiral notch will locate the position of the microstructure most susceptible to cracking.

Implant specimen

The Implant specimen is a Type 304 stainless steel cylinder machined with a spiral notch as shown in Fig. 7(a). Fig. 7(b) is a schematic drawing showing the orientation of the weld cup and implant specimen with respect to rolling direction of the base plate. The specimen would be machined from 0.625 inch thick plate transverse to the direction of rolling. The specimen is approximately 3.5 inches long with a ¼-28 thread on one end and ½-13 thread on the other. The end with the ¼-28 thread was the welded end and the other end connected to the load cell. Table 1 shows the chemical composition of the implant specimen.

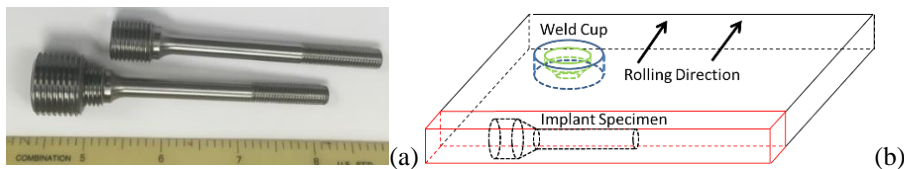


Fig. 7 (a) Photograph showing Implant specimens and adapter collar screwed onto the bottom of the specimens. (b) Schematic drawing showing the implant specimen and weld cup extraction location with respect to base plate orientation.

Table 1 Chemical composition (in weight percent) of Type 304L stainless steel used in this study

Material	C%	Co%	Cr%	Cu%	Mn%	Mo%	N%	Ni%	P%	S%	Si%
304/304L	0.0216	0.1980	18.3105	0.3915	1.8280	0.2855	0.0889	8.1125	0.0325	0.0010	0.2510

Mathematical Modelling of Weld Phenomena 12

Thermal mechanical model

A commercial finite elements software, SYSWELD, was used to model the weld thermal experience and stresses developed during the welding process. This software is also able to predict the resulting weld microstructure as a function of the location on the modelled component. Combining the thermal conditions data with the microstructural evolution history in the specimen, bulk specimens can be created with the targeted microstructural for corrosion susceptibility, pitting-to-cracking transition, fracture mechanics testing, and advanced nondestructive evaluation. These specimens can also be further processed to characterize in-situ corrosion and crack propagation mechanism.

Using as input the welding heat input, physical dimension and geometry of the material, physical material properties, and applying the necessary thermal boundary conditions, SYSWELD was used to model the temperature profiles, microstructure, mechanical properties and the residual stresses developed in the cylindrical specimen.

Model description

Fig. 8 shows the meshed model used in the FEA. The Implant test specimen is constituted of three parts: Base metal, weld metal and the screw. All the three parts are made of type 304 stainless steel; the material properties are chosen from reference [8]. The cross-section view and top view as shown in Fig. 8(a) and Fig. 8(c) depict that the base metal (described earlier also as weld cup) is modeled as a cylinder with a hole created in the middle. This hole is simulated by a cylinder on the top and an inverted cone at the bottom. The screw is connected with the base metal at the bottom of the cone. Welding is conducted on the top of the screw and the weld metal is represented by the brown-colored region. As shown in Fig. 8(d), the top 10 threads in the screw are meshed with very small size elements to clearly describe the most sensitive region under the thermal and mechanical load. Different parts are connected together by the co-node method. The thread is meshed with 4-node tetrahedral elements due to the complicated geometry structure, while the rest is meshed with hexahedral solid elements. The total number of elements is 754,374. The FEA studies for the modified Implant test are conducted using the SYSWELD software.

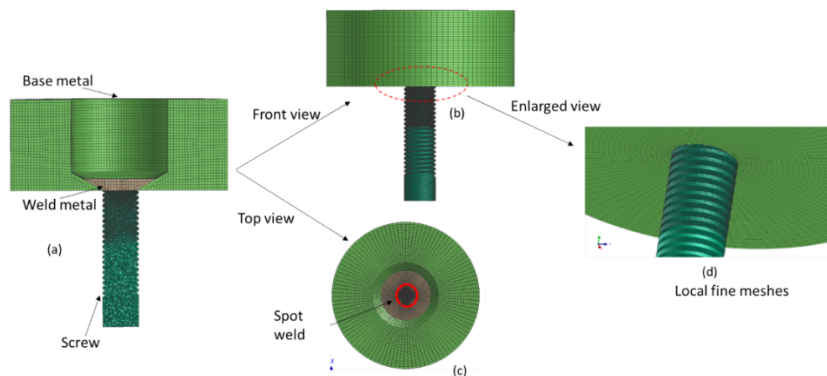


Fig. 8 Meshed model for the modified Implant test simulation. (a) Cross-section view. (b) Front view. (c) Top view. (d) Enlarged view.

Table 2 SYSWELD simulation parameters

Parameter	Welding Current (A)	Welding voltage (V)	Welding velocity (m/s)	Welding time (s)	Cooling time (s)	Tensile load (MPa)
Value	250	32	0.225	4.534	600	170

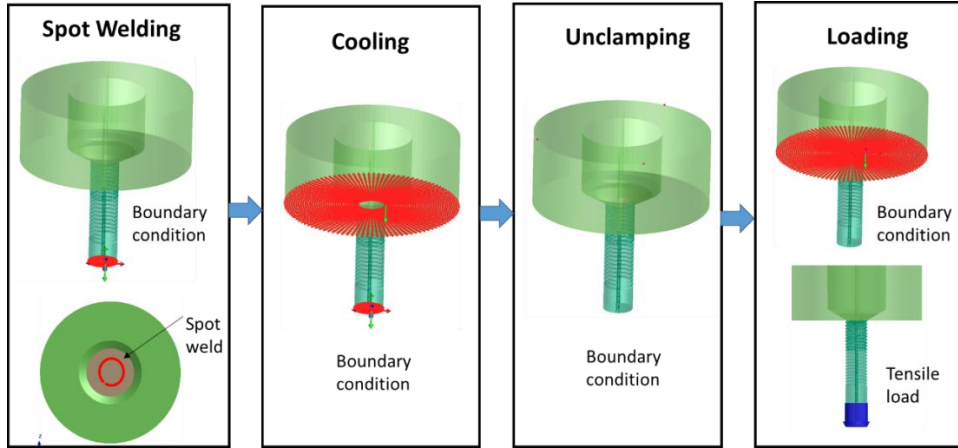


Fig. 9 Schematic drawing showing the progression of welding, cooling, and loading boundary conditions.

The X, Y, and Z directions for the implant specimen shall be defined as the following. The Y direction is the direction in which the specimen is a uniaxial loaded condition, the X and Z directions are transverse to the loading direction. Fig. 9 describes the simulation procedures used in SYSWELD. Firstly, spot arc welding is conducted on the top of the screw; the spot welding is realized following a small circular trajectory. During the welding process, the bottom surface of the screw is fixed. After welding, the three pieces are air cooled for sufficient time. At this stage, the ambient temperature is kept as 20 °C with the bottom surface of the screw fixed. Meanwhile, movement of the base metal in the -Y direction is restricted. Then, after cooling, the whole piece is unclamped with three nodes, during which no thermal or mechanical load is applied. Lastly, a uniaxial tensile load is applied to the bottom surface of the screw. The tensile load value is adjusted to achieve a stress level on the screw to be a fraction of the yield strength of the material (250 MPa). During the loading process, movement of the base metal along the -Y direction is also restricted. By taking the four simulation procedures, a process similar to that observed in the experiment is reproduced on the computer. Table 2 gives the simulation parameters used in SYSWELD. The choice of these parameters is also closely related to the real conditions in experiment.

During the welding process three clamping conditions can arise. The first, both pin and plate (weld cup) are free to expand and contract without restraint during welding or cooling. Second, pin and plate are fixed during welding or cooling. Third, the pin and plate can both move during welding but are fixed during cooling. The third case fits best the intended testing condition. While the specimen is held by the fixture, the pin is free to expand through the hole in the plate upon heating, and the plate is held by gravity to the fixture. Once the

Mathematical Modelling of Weld Phenomena 12

melt pool incorporates both the pin and the plate, and solidification begins, the specimen is deemed as fixed together. As the specimen begins to cool the weld metal has sufficient strength to support the stress in the specimen.

RESULTS AND DISCUSSIONS

WELD RESIDUAL STRESS

Residual stress contours

Fig. 10 summarizes the overall stress contours in the mockup after seven longitudinal weld passes and eight circumferential weld passes. The thermal contraction during solidification and cooling of arc welding induced high tensile residual stress in the weld metals. In the longitudinal welds, as shown in Fig. 10(a), the axial stress is as high as 423.7 MPa in the weld center, which is much higher than the hoop stress. In comparison, a maximum residual stress of 366.1 MPa lies in in hoop direction in the circumferential welds. Both stresses in the two welds are way higher than yield strength (~ 250 MPa), so plastic deformation has initiated. The influence of two intersecting multi-pass weldments on the residual stress distribution is clearly demonstrated in Fig. 10. It should be noted that the highest tensile stress always coincided with the welding direction.

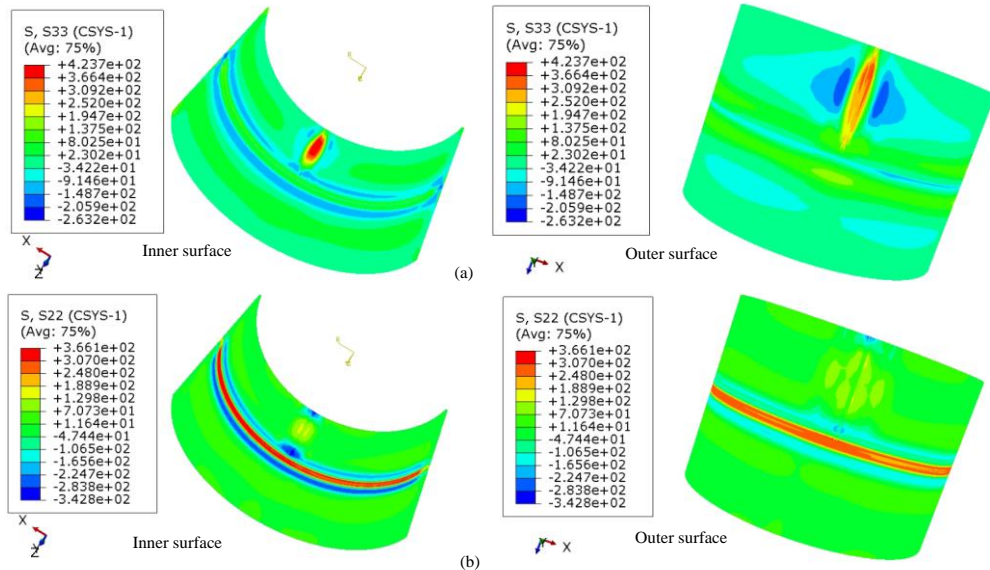


Fig. 10 Overall residual stress contours for (a) axial stress and (b) hoop stress from FEA.

Comparison of FEA with measurement results

Fig. 11 summarizes the residual stress profiles as a function of depth in circumferential weld centerline and HAZ (approximately 4mm away from weld toe on the outer surface) obtained from FEA and DHD measurements, which demonstrates a good agreement. Note that the experimental residual stress data close to the surfaces (≤ 2 mm) were obtained from conventional hole drilling method. Through-wall high hoop tensile stress was observed in the circumferential welds. The maximum hoop stresses in circumferential welds are about 230 to 340 MPa in the weld centerline and approximately 200 MPa in HAZ, respectively. The pre-existing residual stress in the base metal (up to 50MPa indicated by the DHD measurements) induced by the rolling process during manufacturing which was not considered in the FE model, may lead to the difference in residual stress values near surfaces between experimental and simulation results. In comparison, for the longitudinal welds (which is not shown here), high through-thickness axial stresses were observed in the weld metal (320 to 420 MPa) and HAZ (170 to 200 MPa).

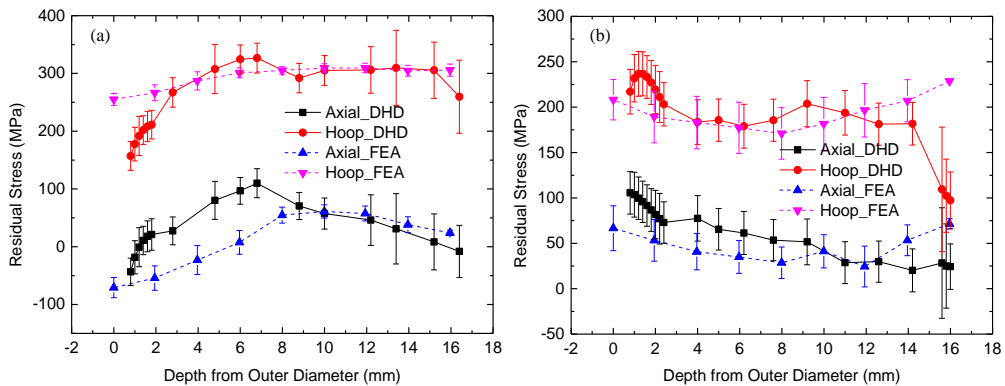


Fig. 11 Residual stress profiles as a function of depth in (a) weld centerline and (b) HAZ of circumferential weld from FE simulation (dashed lines) and DHD measurements (solid lines). The data of FE simulation is averaged from ten points in the steady-state location.

The cross-section stress contour is extracted from FEA results, and compared with the results from contour method for both circumferential and longitudinal weld. Fig. 12 demonstrates the comparison of longitudinal weld. Good agreement is achieved between the FEA and contour measurement results. The residual stresses are strongly tensile through thickness near the longitudinal weld centerline. The simulation result predicts a slightly wider tensile residual stress regime than the contour method, especially on the inner and outer surfaces, which is in agreement with the experimentally observed fusion boundary morphology as illustrated in Fig. 2. Note that tensile stress is observed at the two ends of the welded plate only in the contour method, as shown in in Fig. 12(a), which could be introduced potentially by cutting process.

Mathematical Modelling of Weld Phenomena 12

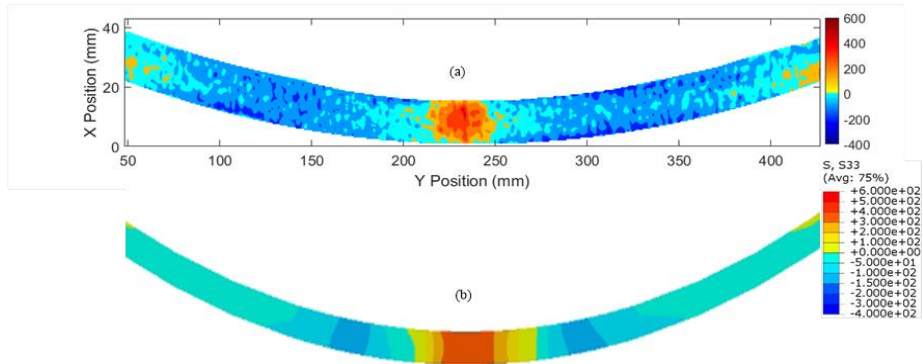


Fig. 12 Cross-section axial stress contour distribution for longitudinal weld from (a) contour method and (b) FEA.

STRESS AND STRAIN DISTRIBUTION OF FOUR-POINT BEND SAMPLE

Verification of FEA results by DIC

The DIC method was able to provide the strain evolution along x axis (//LD, longitudinal weld direction) as a function of displacement load along y axis (//ND, normal direction) in a modified 4PB specimen. The displacement load was carefully applied by turning the two screws in Fig. 5(b) downward slowly and evenly. Good agreement was achieved between the strain profiles obtained from DIC measurement and FEA, as plotted in Fig. 13. As demonstrated by the stress profile, for every 2 mm increase along the thickness direction (y axis), the variation of the stress load would be with a range ± 25 MPa, meanwhile, the constant stress region could extend to around 120 mm along x axis, which could result in a sampling area as $2 \text{ mm} \times 120 \text{ mm}$.

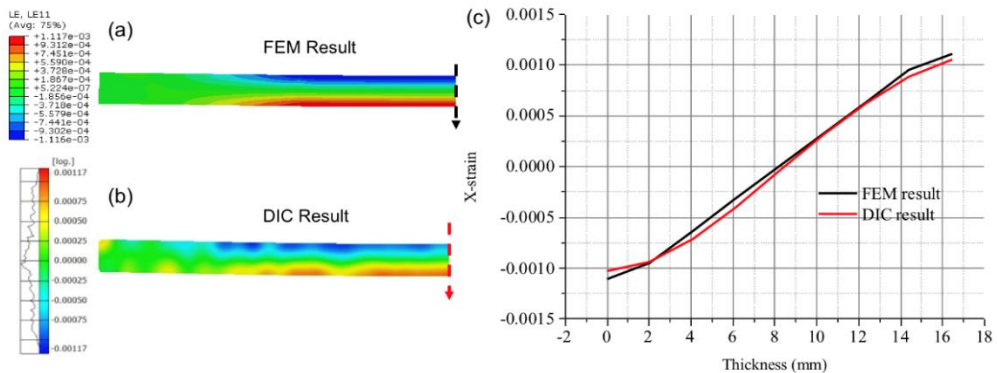


Fig. 13 Comparison of strain contours obtained from (a) FEA and (b) DIC measurement on the modified 4BP specimen, and (c) the strain variations as a function of depth from top surface in the center of the specimen subtracted from the strain maps in (a) and (b).

Mathematical Modelling of Weld Phenomena 12

Stress and strain distributions for the 4pb samples

Fig. 14 gives the strain and stress distributions of the 4PB samples. The DIC method was applied to track the strain evolution during the loading process so as to validate the FEA design. As shown in Fig. 14(a), good agreement was achieved between the strain contour obtained from FEA and DIC measurement. The stress contour was given in Fig. 14(b), which indicates a stress variation from compression to tension along the thickness of the sample. The maximum stress locates at the bottom surface of the sample, which is close to 250 MPa. The stress profile along the thickness in center (Fig. 14(c)) also demonstrates the stress gradient.

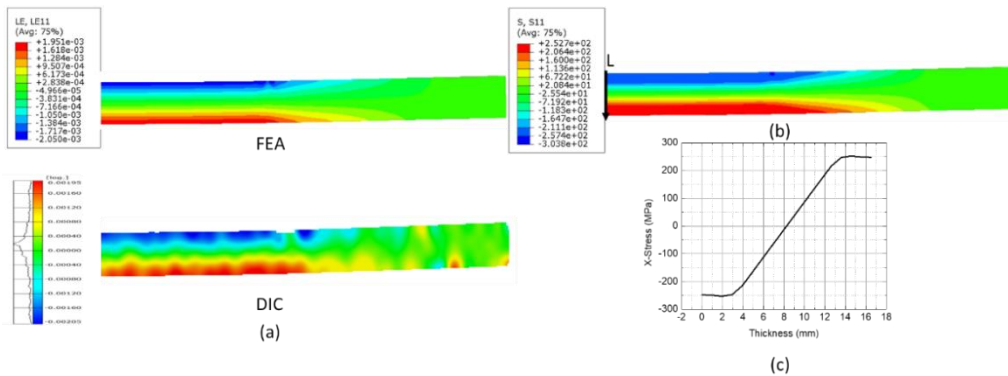


Fig. 14 Strain and stress distribution of the loaded 4PB samples. (a) Comparison of the strain field predicted by FEA and DIC. (b) The stress field predicted by FEA. (c) Stress profile along path L. Only half of the specimen was shown due to symmetry.

THERMAL HISTORY AND SUSCEPTIBLE MICROSTRUCTURES

Fig. 15 is a temperature contour map generated by SYSWELD showing the specimen in 3D and a cross-section of the specimen at the end of the welding time. Fig. 15(b) is a graph showing the temperature profile at the surface of each thread as a function of time. Fig. 16(a) is a photograph showing the root and cap bead of a completed CEMIT specimen before testing. Fig. 16(b) shows a cross section of a tested specimen. The numbering of the threads begins at the toe of the weld and increases as the distance increases, away from the weld. The fusion line is annotated as (FL), weld metal as (WM), heat affected zone as (HAZ), and base material as (BM), respectively. Where the base metal and the weld metal meet on the surface, this location will be referred to as the toe of the weld. Since the weld is actually a melt-through, this location will be referred to as the root of the weld. The fusion line begins internally in the weld cup and exits towards the threads. Note the smooth wetting angle between the threaded portion of the specimen and the weld cup. Fig. 17 is a series of contour maps showing the development in strain and thermal experience. Note that tensile stresses develop between the fusion line and Thread 8. Compression is observed after Thread 8. By matching the actual

Mathematical Modelling of Weld Phenomena 12

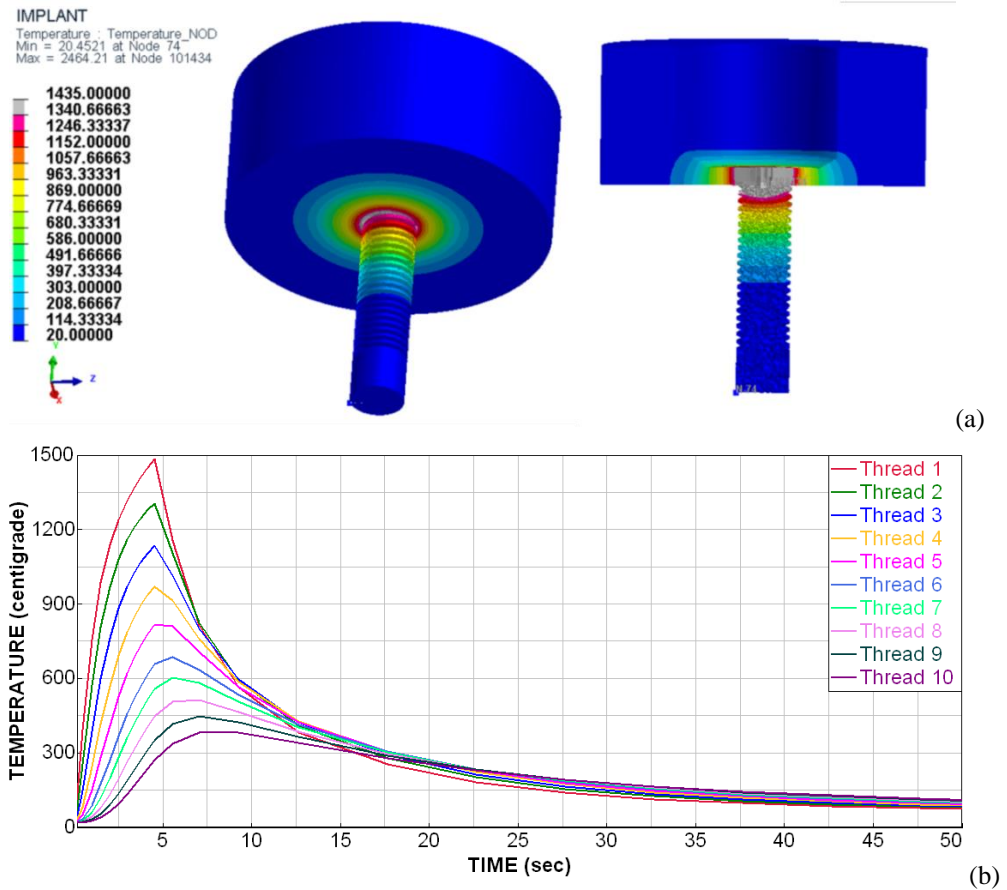


Fig. 15 (a) Temperature contour maps generated by SYSWELD. Graph showing temperature profile at the surface of each thread as a function of time. (b) Simulated time-temperature profiles for each thread generated by SYSWELD.

fracture location observed in the modified Implant test specimens with the SYSWELD calculated temperature contours, the region where the microstructure was most sensitive to cracking could be identified. Fig. 17(a) show the stress contour maps of the specimen upon release from the fixture after cooling, with clear indication that the specimen is loaded during testing. Note the regions in Threads 5 to 8 that does not stress to the same levels as the upper portions of the threads. High surface and subsurface tension in the specimen close to the fusion line may promote crack opening in this region if the microstructure is predisposed to cracking. Thus, it is important to match the microstructure with the developed stresses to confirm the effect of sensitization. Fig. 17(b) shows the stress contour within the specimen after unloading and then the stress reapplied to 170 MPa. Note that while loading the stress applied is below the yield stress, the stress levels within the first 7 threads reach a level at or above the yield strength due to the residual stresses. This is important since the actual welds within the canister also have residual stress.

Mathematical Modelling of Weld Phenomena 12

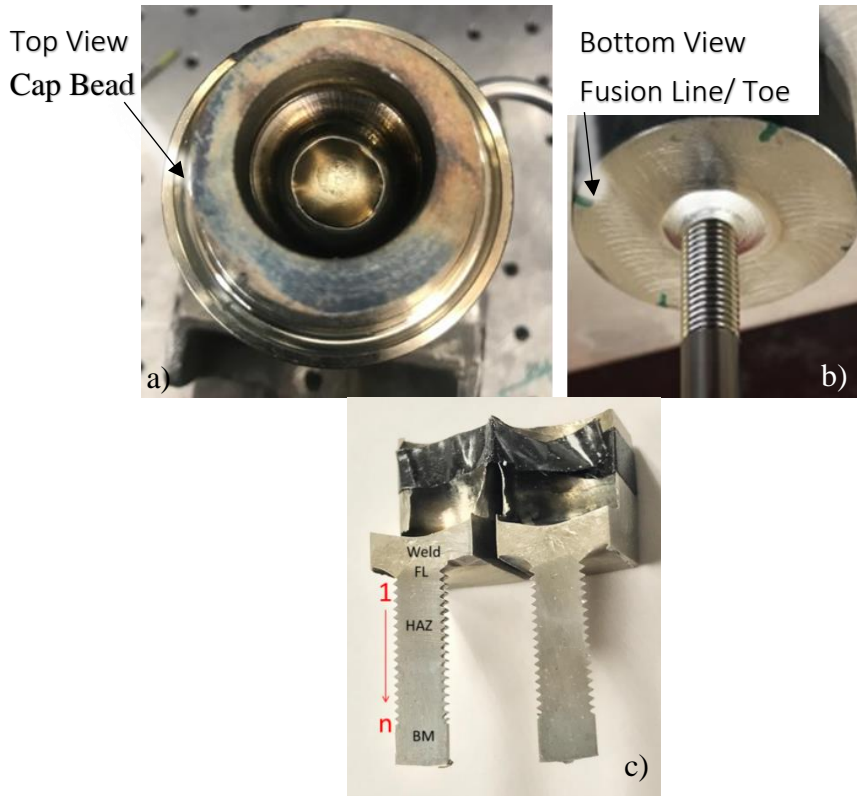


Fig. 16 (a) Photographs showing a completed weld with acceptable appearance viewed from both the top into the weld cup and from the bottom with threaded test region and weld root in view. (b) Photograph showing the cross-section of a completed weld. The weld threads have been numbered beginning at the fusion line and increasing in number as the base material is approached. The weld, fusion line (FL), heat affected zone (HAZ) and base metal (BM) are labelled. Where the base metal and the weld metal meet on the surface, this will be referred to as the toe of the weld. The HAZ is between the fusion line and the base material. This is the region where sensitization occurs. The BM is the material which is unaffected by any processing.

Several implant specimens were produced and tested. Minor corrosion and cracking were observed throughout all of the specimens, and in particular at the base of the threads, the fusion line, and in regions where residual stress and cold work were produced during the machining process. Observation showed that corrosion and SCC occurred in the HAZ, between Threads 5 and 10, which correspond well with the region that experienced between 450 to 850 °C as predicted by the software. Fig. 18 shows two SEM images of the CEMIT specimen. Fig. 18(a) is an image taken at 23x showing indications of corrosion in Threads 6 to 8. Fig. 18(b) is an SEM photograph taken from the cross-section of the same implant specimen in Thread 7. A crack can be observed splitting the grain boundary between the austenite (light color) and the delta Ferrite (darker color). Since the initial processing conditions for wrought 304L includes a water quench, it is reasonable that small amounts of delta ferrite remain in the base material. Using a Feritscope and SEM, it was confirmed that ferrite was present. Small precipitates and carbides were observed decorating the grain

Mathematical Modelling of Weld Phenomena 12

boundary. As shown in Fig. 15(b), Thread 7 reached a peak temperature just below 600 °C. This condition was consistent with that needed for the nucleation and growth of the $M_{23}C_6$, thus leading to sensitization and potentially, SCC. The formation of the $M_{23}C_6$ was verified by performing a selective digestion method and then analysed using XRD. Further verification was performed by creating carbon extraction replicas and observing the precipitates using TEM. The carbides were observed in the etch pits and decorating the grain boundaries. It was found that the carbide morphology was consistent with literature and EDS results were reasonable. While a kinetic model would help to show that favourable conditions existed for the formation of the carbides, this was not the focus of this study. Future work should and will include this type of model.

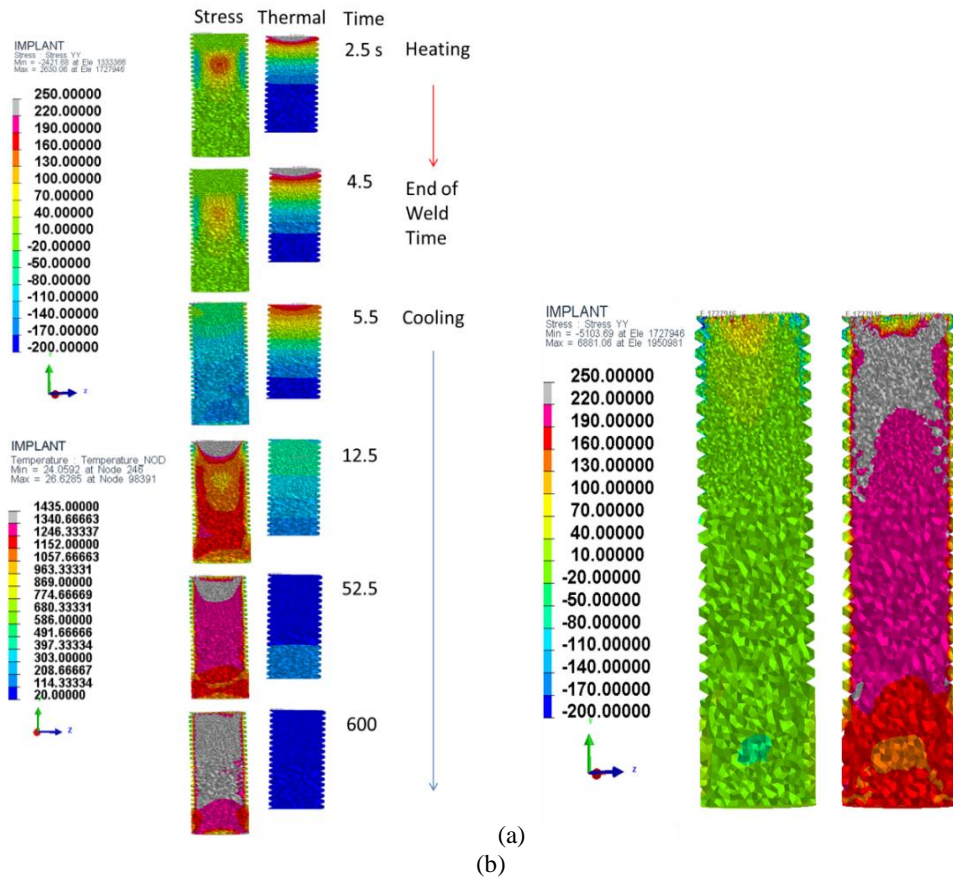


Fig. 17 (a) Contour maps showing the development in strain and thermal experience (temperature history) along the screw. (b) Stress contour map showing the specimen after welding (L) and upon release from the fixture (R) showing the stress developed upon reloading to 170 MPa.

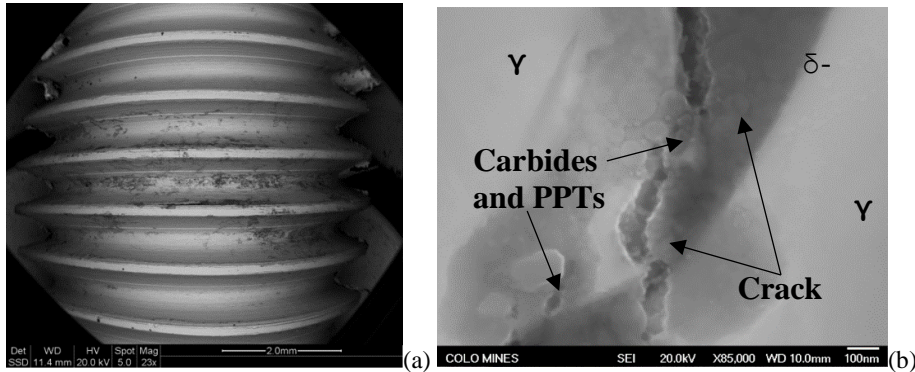


Fig. 18 (a) SEM image taken at 23X magnification showing corrosion on Threads 5 to 9 from top to bottom. (b) SEM micrograph taken at 85000x showing a crack propagating through the boundary between ferrite and austenite. Note the small carbides decorating the grain boundary.

CONCLUSIONS

From the numerical studies performed on the canister welding, 4PB test and CEMIT, it was concluded that:

- (1) Based on the thermal and stress results of the CEMIT predicted by the FEA model, the crack initiation site observed in the microscope can be clearly explained. These numerical studies could offer important information about the susceptible microstructure and tensile stresses for the canister, which is meaningful for the future investigation of the initiation and growth rate of CISCC.
- (2) The canister simulation was validated by measured stress data obtained using deep-hole drilling and contour methods. High through-thickness hoop stresses were found within the weld metal (230 to 340 MPa) and HAZ (approximately 200 MPa) in circumferential welds. In comparison, high through-thickness axial stresses were observed in the weld metal (320 to 420 MPa) and HAZ (170 to 200 MPa) in longitudinal welds.
- (3) A 4PB test setup was reasonably designed by FEA and DIC to duplicate the stress conditions in the mockup canister. For every 2mm increase along the thickness direction, the variation of the stress load would be with a range ± 25 MPa, which could result in a sampling area as 2 mm \times 120 mm.
- (4) Corrosion and cracking was observed in the CEMIT process concentrated within threads 5 to 9. This region falls within the temperature range suitable for the precipitation of the $M_{23}C_6$ carbides. The combination of this sensitized microstructure, a sufficient load, and the corrosive environment lead to fracture in the CEMIT specimen.

Mathematical Modelling of Weld Phenomena 12

ACKNOWLEDGEMENTS

This work was supported by the DOE, Nuclear Engineering University Program (NEUP) under grand number DE-NE0008442 of Integrated Research Program (IRP), no. IRP-15-9318. The authors would like to gratefully acknowledge ESI Group for making the SYSWELD software available to the researchers of the Center for Welding, Joining and Coatings Research of the Colorado School of Mines. Their technical support and discussion are also kindly appreciated.

REFERENCES

- [1] R. M. KAIN: 'Marine Atmospheric Stress Corrosion Cracking of Austenitic Stainless Steels', *Materials Performance*, Vol. 29, No. 12, pp. 60-62, 1990.
- [2] D. G. ENOS, C. R. BRYAN and K. M. NORMAN: 'Data Report on Corrosion Testing of Stainless Steel SNF Storage Canisters', *FCRD-UFD-2013-000324*, U.S. Department of Energy, Office of Used Nuclear Fuel Disposition, 2013.
- [3] C. R. BRYAN and D. G. ENOS: 'Analysis of Dust Samples Collected from Spent Nuclear Fuel Interim Storage Containers at Hope Creek, Delaware, and Diablo Canyon, California', *SAND2014-16383*, Albuquerque, NM, Sandia National Laboratories, 2014.
- [4] C. R. BRYAN and D. G. ENOS: 'Analysis of Dust Samples Collected from an Unused Spent Nuclear Fuel Interim Storage Container at Hope Creek, Delaware', *SAND2015-1746*, Albuquerque, NM, Sandia National Laboratories, 2015.
- [5] A. KOSAKI: 'Evaluation method of corrosion lifetime of conventional stainless steel canister under oceanic air environment', *Nuclear Engineering and Design*, Vol. 238, No. 5, pp. 1233-1240, 2008.
- [6] NUCLEAR REGULATORY COMMISSION (NRC): 'Finite Element Analysis of Weld Residual Stresses in Austenitic Stainless Steel Dry Cask Storage System Canisters', *NRC Technical Letter Report (ADAMS ML13330A512)*, Washington, D.C., 2013.
- [7] D. G. ENOS and C. R. BRYAN: 'Characterization of Canister Mockup Weld Residual Stresses', *FCRD-UFD-2016-000064*, *SAND2016-12375 R*, Albuquerque, NM, Sandia National Laboratories, 2016.
- [8] D. DEAN and M. HIDEKAZU: 'Numerical simulation of temperature field and residual stress in multi-pass welds in stainless steel pipe and comparison with experimental measurements', *Computational Materials Science*, Vol. 37, No. 3, pp. 269-277, 2006.
- [9] C. LIU, J. X. ZHANG and C. B. XUE: 'Numerical investigation on residual stress distribution and evolution during multi-pass narrow gap welding of thick-walled stainless steel pipes', *Fusion Engineering and Design*, Vol. 86, No. 4-5, pp. 288-295, 2011.
- [10] J. GOLDAK, A. CHAKRAVARTI and M. BIBBY: 'A new finite element model for welding heat sources', *Metall Trans B*, Vol. 15, No. 2, pp. 299-305, 1984.
- [11] X. WU, Z. YU: 'Final Report: Weld Residual Stress Analysis in the Canister Mockup', *DE-NE0008442 of Integrated Research Program No. IRP-15-9318*, Golden, CO, Colorado School of Mines, 2018.
- [12] H. GRANJON: 'The Implants Methods for Studying the Weldability of High Strength Steels', *Metal Construction and British Welding Journal*, Vol. 1, No. 11, pp. 509-515, 1969.
- [13] J. M. SAWHILL, JR., A. W. DIX, W. F. SAVAGE: 'Modified Implant Test for Studying Delayed Cracking', *Welding Journal*, Vol. 53, No. 12, pp. 554-s-559-s, 1974.